ELSEVIER

Contents lists available at ScienceDirect

Colloids and Surfaces B: Biointerfaces

journal homepage: www.elsevier.com/locate/colsurfb





Sol-gel coating loaded with inhibitor on ZE21B Mg alloy for improving corrosion resistance and endothelialization aiming at potential cardiovascular application

Weijie Li^{a,b}, Ya Su^b, Liang Ma^{a,b}, Shijie Zhu^{a,b}, Yufeng Zheng^d, Shaokang Guan^{a,b,c,*}

- ^a School of Materials Science and Engineering, Zhengzhou University, Zhengzhou 450001, China
- ^b Henan Key Laboratory of Advanced Magnesium Alloys, Zhengzhou 450002, China
- ^c Key Laboratory of Advanced Materials Processing & Mold Ministry of Education, Zhengzhou 450002, China
- d College of Engineering, State Key Laboratory for Turbulence and Complex System, Department of Materials Science and Engineering, Peking University, Beijing 100871,

ARTICLE INFO

Keywords: Magnesium alloy Self-healing Corrosion inhibitor Coatings Anticoagulation

ABSTRACT

To improve the service performance of vascular stents, we designed/selected a series of organic compounds from commercial drugs, natural plants, and marine life as the potential corrosion inhibitors for ZE21B alloy. Paeonol condensation tyrosine (PCTyr) Schiff base was found to be the most efficient inhibitor among them. The biocompatible, self-healing, anti-corrosive sol-gel coating loaded with corrosion inhibitor was fabricated on the Mg substrate through a convenient dip-coating tactic. The corrosion resistance, self-healing ability, cytotoxicity, and hemocompatibility of the coated sample were evaluated. These results suggested the potentiality of Schiff base inhibitor-loaded sol-gel coating for enhanced corrosion protection and desired biocompatibility of bio-absorbable cardiovascular implants.

1. Introduction

In view of its excellent biocompatibility and biodegradability, magnesium alloy can become one of the strong competitors of vascular stent materials. However, its relatively fast degradation rate has become a huge barrier for the popularization and application of biological magnesium alloys. In order to solve this problem and achieve controllable degradation, scientists have made a lot of attempts. To sum up, there are mainly three methods to improve the corrosion resistance of magnesium alloys. The first method is to optimize the design of magnesium alloy, in addition to the common WE43 [1] and AZ31 [2], based on the influence of electronegativity and toxicity of alloy elements, the ZE21B alloy (ZE21B) [3,4], Mg-Nd-Zn-Zr alloy (EK20M) [5,6] have been widely reported. The second solution is surface modification of magnesium alloy. Such as micro-arc oxidation (MAO) [7], polymer coatings [8,9], silanization [10], and their composite coatings [11-14], etc. However, in clinical practice, stent implantation needs deformation such as gripping and expansion, which will inevitably damage the stent coating and cause microcracks or micro warpage, corrosion will start from the damaged area of the coatings, which will lead to the failure of implant operation

or premature failure of the stent during the service period. The third method is to add corrosion inhibitors into the specific application system of magnesium alloy. For example, glucosamine sulphate [15], L-Tyrosine [16], and salicyl hydroxamic acid [17]. Still the use of corrosion inhibitor requires a relatively closed environment.

The above three solutions have certain limitations when used alone. Some scholars put forward the method of combining corrosion inhibitor with coating. It is found that the coating loaded with corrosion inhibitor has a self-healing [18–21]effect, which can better control the degradation of magnesium alloy at a specific rate. In light of this, a series of corrosion inhibitors [22–37] for magnesium alloys have been designed, However, most of them are toxic, harmful, non-degradable, or not suitable for the physiological environment. Therefore, the key to the preparation of self-healing coating is to find a high-efficiency, non-toxic, and bioactive corrosion inhibitor for magnesium alloy.

As a magnesium alloy vascular implant, in addition to the controllable degradation of the coating design, the blood compatibility and endothelialization of the surface should also be considered, the most common method is to coat the coating with drugs such as paclitaxel [38], rapamycin [39,40], and sirolimus [41]. If we can design a

^{*} Corresponding author at: School of Materials Science and Engineering, Zhengzhou University, Zhengzhou 450001, China. E-mail address: skguan@zzu.edu.cn (S. Guan).

compound that can not only inhibit corrosion but also replace the above drugs to be coated in the coating, then the coating can achieve self-healing, rapid endothelialization, improved biocompatibility, and other functions at the same time, and it will be more suitable for magnesium alloy vascular stent.

In this work, we designed/selected a series of organic compounds from commercial drugs, natural plants, marine life, and their derivatives as the potential corrosion inhibitors for ZE21B alloy. Based on the weight loss results, the most efficient one, PCTyr Schiff base, was screened out. Afterward, it was incorporated into sol-gel (TEOS/GPTMS) to fabricate an anti-corrosive and biocompatible coating on ZE21B alloy. The degradation property of the coated sample was investigated by electrochemical and immersion tests. The scratch test, AFM measurement, water contact angle, toxicological assays, and hemocompatibility were employed to investigate the service properties of the coated samples.

2. Materials and methods

2.1. Materials

Cylindrical discs ($\Phi 10 \times 4$ mm) samples were mechanically cut from CEC ZE21B (Mg-2.0Zn-0.5Y-0.5Nd, wt%) alloy bar. Before each experiment, the ZE21B discs were polished step by step with silicon carbide grinding papers and then sealed with resin, leaving only the working face for use. 3-Glycidoxypropyltrimethoxysilane (GPTMS, Aladdin reagent, China, 97 %) and tetraethoxysilane (TEOS, Aladdin, China) were used as precursors for synthesizing the hybrid matrix sol.

2.2. Comprehensive screening of corrosion inhibitors

An immersion test was employed to comprehensively screen potential corrosion inhibitors. The chemical structure of all tested compounds is presented in Table 1. Due to the poor solubility of Curcumin and Quereetin in an aqueous solution, Curcumin powder was firstly dissolved in ethanol to enhance the compatibility of Curcumin in the saline solution; Quereetin was chemically modified to water-soluble Quereetin-5'-sulfonic acid according to a published procedure [42]. PCTyr Schiff base was synthesized by Paeonol and tyrosin according to the literature [43] and characterized by IR analysis. An immersion test was performed in the blank solution (saline solution, 0.9 wt.% NaCl) and inhibitor-containing solutions. Although NaCl solution could not reflect the complexity of the real body fluids, it was selected here to provide the harsh environment to test the inhibition efficiency $(\eta_{\mathbf{w}})$ of the potential inhibitors [44]. The duration of immersion was 3 days.

$$\eta_w = \frac{V_0 - V_1}{V_0} \times 100\%$$

where v_0 and v_1 are the average weight loss corrosion rates in the blank solution and an inhibitor containing solution, respectively.

2.3. Sol synthesis and preparation of the self-healing coatings

The silane sol was synthesized by mixing GPTMS and TEOS (molar ratios = 5:1), the solvent is an appropriate amount of distilled water and ethanol. Followed stir the solution for 30 min to make it mix well, the solution was hydrolyzed for 1 h by adding acetic acid (0.3 M) to adjust pH = 4.5. Then the right amount of ammonia (0.5 M) was added to accelerate the condensation reaction. The above solution was doped with corrosion inhibitor (PCTyr Schiff base), then aged for 24 h. The dipping technique was used for preparing coatings using a withdrawal speed of 1 mm/s. The coated samples were thermally cured at 60 $^{\circ}$ C for 3 h.

Table 1
Inhibiting efficiency of all tested compound for ZE21B alloy.

Chemical compound	Structural formula	Concentration	$\eta_{\rm w}\%$
Curcumin	o o d d d o o	0.004 mM	53.9
Quereetin- 5`-sulfonic acid	HO OH OH	1 mM	36.8
Aspirin	OH OH	0.1 mM	26.8
Sodium alginate	Naccoc HO Naccoc	1000 ppm	13.5
Hematoxylin	HO COONS OH	0.3 mM	45.4
Paeonol	NO N	1 mM	31.0
PCTyr Schiff base	ОН	3 mM	79.2
Chondroitin sulfate	HO O OH OH	0.01 g/mL	44.4
Edaravone	NN OH	0.26 mM	28.3
Taurine	ОН	1 mM	-82.5
Paracetamol	H ₂ N OH	1 mM	5.3

2.4. Surface characterization

The surface morphologies of samples were observed by a SEM (FEI Quanta-200, USA). The chemical structures of the samples were confirmed by Fourier transform infrared spectroscopy (Nicolet 6700, USA). The surface roughness of the coating sample was characterized by an atomic force microscope (SPMQ500-J3, Japan). Wetting properties of uncoated and coated samples were determined by a contact angle meter (SL 2005KS, China).

2.5. Degradation characterization

The corrosion behavior of the samples was also examined by static immersion test according to ASTM G31 in Simulated Body Fluid (SBF) [44]. The chemical compositions of degradation products were analyzed

using EDS. The potentiodynamic polarization and electrochemical impedance spectra of electrochemical tests were carried out using a classical three electrodes cell in SBF. The specific operation steps are shown in the published literature [45] of the research group.

2.6. Evolution of self-healing property

Scratch tests were performed to evolution the self-healing property of each sample. The preparation and testing of scratch specimens are similar to the literature [46]. Then put the scratched samples in SBF solution at 37 $^{\circ}$ C immersed within a certain time frame to allow self-healing.

2.7. Endothelial cells culture

Choose Human Umbilical Vein Endothelial Cells (HUVEC, Haoyi Biotecholygy Co., Ltd., Chengdu, China) of 3rd to 5th passages were selected as the experiment subjects. The cytotoxicity was determined by MTT assay. The bare ZE21B, sol-gel ZE21B and PCTyr chiff base sol-gel ZE21B samples were put into 24 well plate and soaked in pure culture medium for 24 h to obtain the sample extract. HUVECs were seeded in 96 well plate at the density of 2×10^4 cells/mL, and the pure medium was set as reference. After 24 and 72 h of culture, MTT solution was added and then cultured for 4 h, the waste liquid was removed and DMSO was added. The OD value of absorbance value of each orifice plate was determined by enzyme standard instrument at 492 nm wavelength.

The HUVEC were seeded onto the 24 well plate with the concentration of 1.5×104 cells/mL, after incubation at 37 °C for 1 day, the sample extract was added. After the sequentially washed step, the samples were fixed with 4% paraformaldehyde (Sigma, USA) for 2 h at room temperature and stained by rhodamine reagent for 15 min, following with DAPI for 5 min, finally examined and recorded by a fluorescence microscope [47].

HUVECs migration of each sample was studied by physical scratch method. The pipet tips were used to leave a scratch on each sample. After incubation for 18 h and 36 h, the migration of each sample was evaluated by calculating the variation of scratch width, respectively [48].

2.8. Blood compatibility

The blood compatibility was evaluated by platelet adhesion and hemolysis tests.

Platelet adhesion: The fresh blood was donated by volunteers, and sodium citrate was added as an anticoagulant. The samples and the control group were placed in the extracorporeal flow chamber device, the equipment parameters were set to 37 $^{\circ}\text{C}$, and the blood flowed at a speed of 45 dyn/cm² for 1 h. Then, the sample was taken out, washed three times with PBS for five minutes each time, and then fixed with a 2.5 % glutaraldehyde solution at 4 $^{\circ}\text{C}$ 2 h and washed with ultrapure water. Finally, ethanol solutions (50 %, 75 %, 90 %, 100 %; Valcohol/ Vwater) were used to gradient dehydrate samples for the following characterizations. All the sample was dried at the critical point of CO₂, and then the surface of the sample was sprayed with gold and observed by SEM.

Hemolysis tests: Use 20 g/L sodium citrate solution as an anticoagulant, and add 0.5 mL of fresh blood from healthy volunteers was added with normal saline and mixed to prepare 10 mL of diluted blood. According to international standard (IS010993.4:2002), different samples to be tested were immersed in test tubes containing 10 mL of normal saline (experimental group), and 3 parallel samples were set for each group. All the tests were maintained at 37 $^{\circ}$ C for 30 min. Then take 10 mL of distilled water (positive control group) and 10 mL of normal saline (negative control group), and add 0.2 mL of diluted blood to each test tube. Then all the test tubes were kept at 37 $^{\circ}$ C for 60 min, and then the

media were taken out and centrifuged at 2500 r/min for 5 min. Finally, a spectrophotometer (722, Shanghai Precise Science Instrument, China) was used to measure the absorbance value at a wavelength of 545 nm. All the measurements were repeated at least three time for confirming the reproducibility. [47].

2.9. Statistical analysis

Every test was carried out three times, statistical significance requires a p-value <0.05.

3. Results and discussion

3.1. Inhibitor screening results

In past decades, scientific workers devoted to developing corrosion inhibitors to retard the corrosion of magnesium, particularly systematical studies about a comprehensive screening of Mg corrosion inhibitors and concept for corrosion inhibition of magnesium have been performed by Lamaka et al. [49–52]. Base on the newly proposed concept, suppression of iron re-deposition, the presents the results of systematic screening for magnesium corrosion inhibitors. The inhibiting effect of 151 individual compounds was tested towards six alloys (AZ31, AZ91, AM50, WE43, ZE41, and Elektron 21) and three grades of pure magnesium. Salicylate, fumarate and prydrinedicarboxyliate were proven to be highly efficient corrosion inhibitors. However, their work mainly focuses on the engineering application of magnesium corrosion inhibitors, the biocompatibility of the potential inhibitors was not considered seriously.

In this work, we selected the potential inhibitors from the natural compounds, which probably have better biocompatibility. Combined with the Langes Handbook of Chemistry (70th-Anniversary-Edition) and published literature, it could be found that the cumulative formation constants for magnesium with inorganic ligands (log K) are an important index for magnesium inhibitor screening in the Table of supplementary material. Therefore, several organic compounds from natural compounds or their derivatives (Curcumin, Quereetin-5-sulfonic acid, Sodium alginate, Hematoxylin, Paeonol, Chondroitin sulfate), medicine in stock (Aspirin, Edaravone Injection, Paracetamol, Taurine) might be the potential corrosion inhibitors for Mg alloys owing to their chelating effect. As shown in Table 1, it could be found that most of these compounds showing inhibition efficiency except for Taurine under a certain doping content. (It should be noted that most of the tested compound concentrations are based on the similar chemical structure used for magnesium alloy, aluminum alloy, or other alloys given in the references.) Taurine shows a negative value, which means that it accelerates Mg corrosion. It is reasonable since magnesium taurate, the reaction product between Taurine and Mg in the saline solution, is water-soluble [53]. It cannot be deposited on the magnesium surface to prevent the attack of chloride ions. The inhibition efficiency of Curcumin, Hematoxylin, PCTyr Schiff base and Chondroitin sulfate are all greater than 40 %. In particular, the inhibition efficiency of PCTyr Schiff base was 79.2 %, which is three times more than that of its reaction substrate, Paeonol. In summary, it could be speculated that the compounds which have relatively higher stability constant with Mg²⁺ and the corresponding chelates that have less solubility may be highly efficient inhibitors.

Based on the inhibition efficiency, as well as the comprehensive consideration of solubility, biocompatibility, and chemical structure stability, etc., PCTyr Schiff base was selected as the best one from all test compounds. Fig. 1 shows SEM images of magnesium alloy after 3 days' immersion in normal saline with or without PCTyr Schiff base. It has a loose flocculent structure from the sample in a normal saline solution (Fig. 1A). However, the corrosion products formed in PCTyr Schiff base-containing solution show compact and regular spherical structure (Fig. 1B). After removing the corrosion products, serious pitting and some cracks can be observed on the specimen surface which immersion

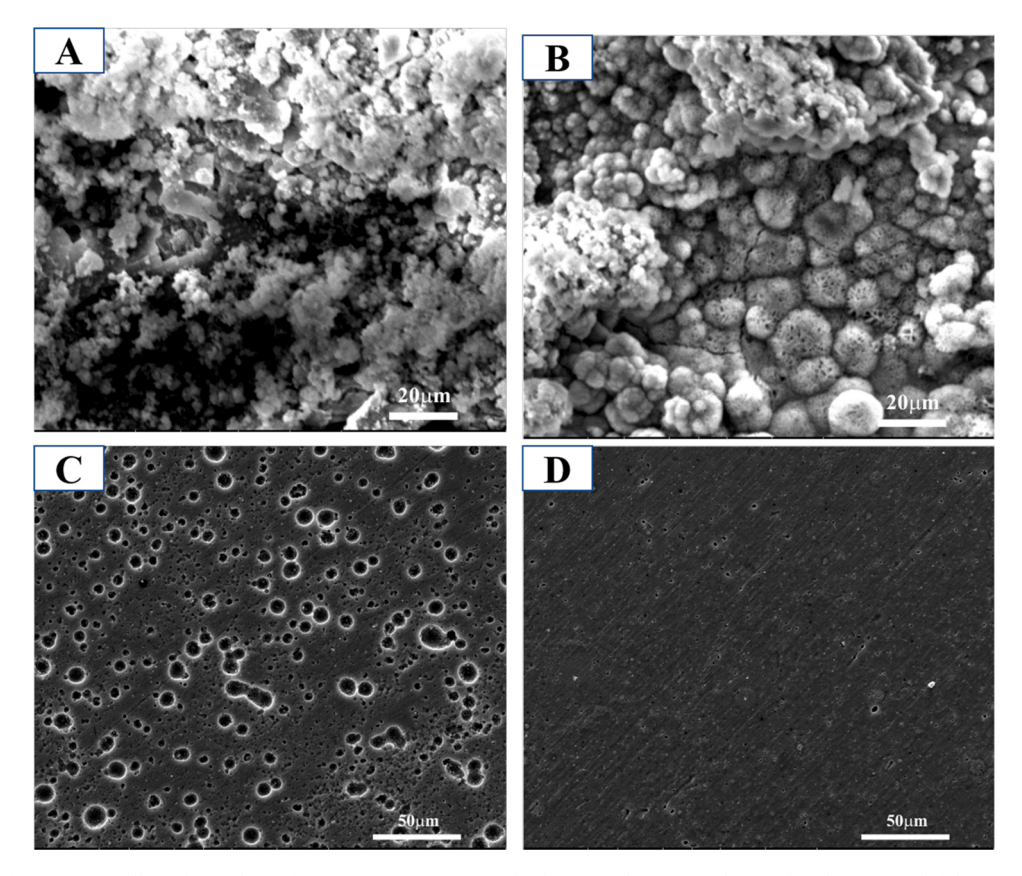


Fig. 1. SEM images of magnesium alloy after 3 days of immersion in 0.9 % NaCl solution without (A and C) and with PCTyr Schiff base (B and D). (Aand B with corrosion products), (C and D are after removal of corrosion products).

in blank solution (Fig. 1C), but the surface in the inhibitor-containing solution is smooth and less severe corrosion (Fig. 1D). Obviously, the PCTyr Schiff base not only decreases the corrosion rate of Mg but also makes Mg corrosion more uniform. The further parameter optimization and inhibition mechanism of the PCTyr Schiff base inhibitors have been introduced in our published literature [54].

3.2. Surface characterization of coating

Fig. 2 shows FT-IR spectra of coatings where the O—H absorption bands, associated with the presence of solvent/water, can be observed at 3390 and 1649 $\rm cm^{-1}$. It should be noticed that the 1096 $\rm cm^{-1}$ of the stretching vibrations bands concerned to the Si-O-C groups, and

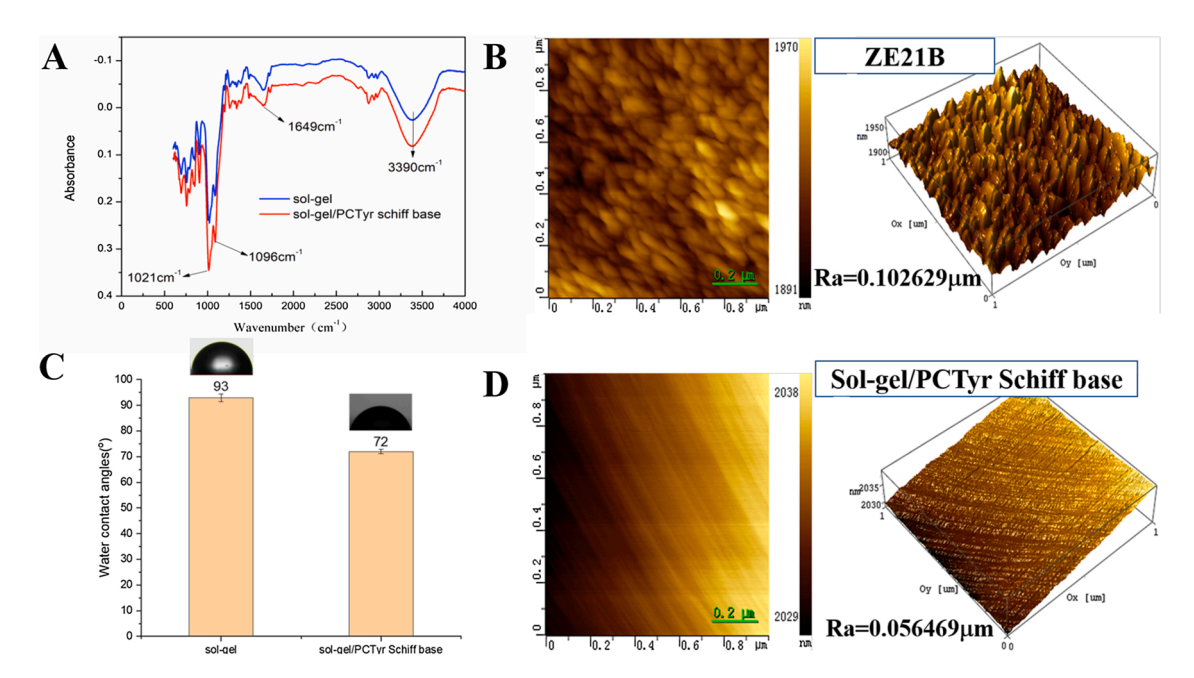


Fig. 2. A FTIR spectra of the sol-gel (TEOS-GPTMS) and PCTyr Schiff base sol-gel coatings; B Coating surface roughness 3D morphology (ZE21B); C Water contact angle of coatings; D. Coating surface roughness 3D morphology (PCTyr schiff base sol-gel coating).

characteristic Si-O-Si band at 1040 cm⁻¹ [55] attributed to the condensation reaction was also observed. The characteristic C—N stretching vibration absorption of PCTyr Schiff base was also at 1600 cm⁻¹, which coincides with the O—H absorption bands characteristic peak(1649 cm⁻¹). Thus, the general trend of FT-IR spectra for PCTyr Schiff base sol-gel is similar with that of the sol-gel coating, and there was no new characteristic peak appeared. This result also indicates that there is no obvious chemical reaction between the loaded Schiff base and sol-gel coating. In other words, the corrosion inhibitor and sol gel coating can coexist harmoniously.

The evaluation of roughness is usually expressed by Ra, the smaller the Ra value is, the smoother the surface of the sample. As shown in Fig. 2B and D, the Ra of PCTyr Schiff base sol-gel coating (0.056469 $\mu m)$ is smaller than that of the ZE21B matrix (0.102629 $\mu m)$. The possible reason is that the Schiff base inhibitor is weakly alkaline, and its addition is more conducive to the cross-linking of silane and, thus, making the coating more compact and smoother.

The contact angle of the two coatings is shown in Fig. 2C. The contact angle of sol-gel coating is 93°, which appears slightly hydrophobic

because the silane coupling agent contains some hydrophobic carbon chains after the condensation reaction. The contact angle of the PCTyr Schiff base loaded sol-gel coating is 72° , which is lower than that of the sol-gel coating. It could be attributed to the presence of hydrophilic hydroxyl and carboxyl groups in the loaded PCTyr Schiff base.

3.3. In vitro degradation behavior

3.3.1. Electrochemical test

Electrochemical testing is a rapid measure of corrosion or degradation of metal materials. Tafel plots of various ZE21B samples are revealed in Fig. 3A (a). Electrochemical parameters obtained from measured polarization curves were shown in Table 2. The $E_{\rm corr}$ value of PCTyr Schiff base sol-gel sample (-1.6574 V) and sol-gel sample (-1.6467 V) less negative than the bare ZE21Bsample (-1.7356 V), implying retard of corrosion. The $I_{\rm corr}$ value of PCTyr Schiff base sol-gel sample (3.64E-06) and sol-gel sample (4.29E-06) are two orders of magnitude lower than that of the substrate (1.31E-04). Generally speaking, $I_{\rm corr}$ is an important indicator of corrosion rate, the smaller the $I_{\rm corr}$ is, the better

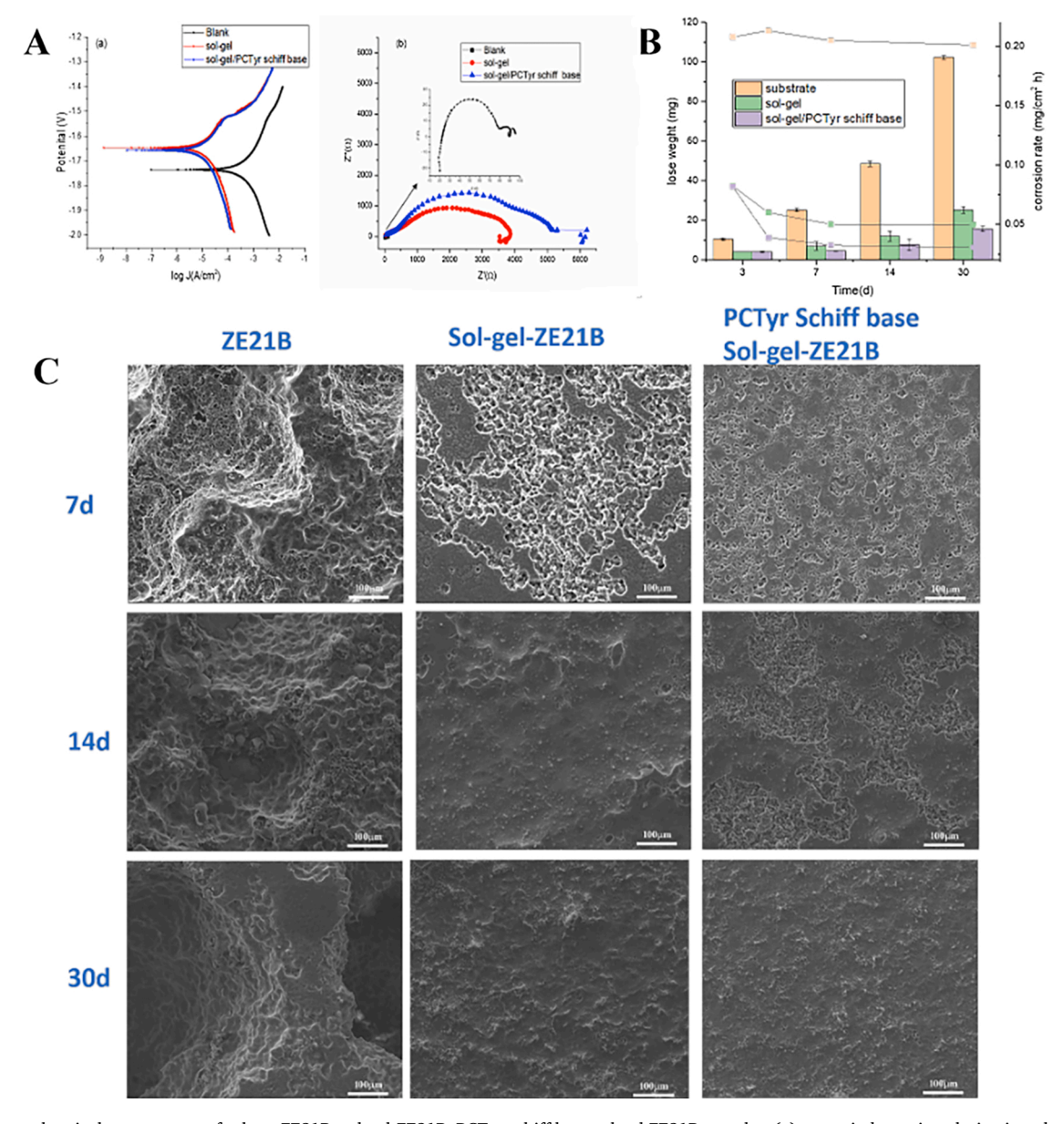


Fig. 3. A Electrochemical measurement for bare ZE21B, sol-gel-ZE21B, PCTyr schiff base sol-gel ZE21B samples: (a) potentiodynamic polarization plots; (b) Nyquist plots; B In vitro immersion tests of the coatings over 30 days at 37 °C in SBF; C Surface morphology of the samples at 37 °C in SBF.

 Table 2

 Electrochemical parameters obtained from measured polarization curves.

Samples	b _a (mv/dec)	b _c (v/ dec)	I _{corr} (A/cm ²)	E _{corr} (V)
Substrate	71	0.074	1.31E-04	-1.7356
sol-gel	71	0.075	4.29E-06	-1.6467
sol-gel/ PCTyr schiff base	69	0.072	3.64E-06	-1.6574

the corrosion resistance of the coating. It shows that the two coatings have a certain protective effect on the magnesium alloy substrate, and the loading of the PCTyr Schiff base further improves the corrosion resistance of the coatings. Nyquist plots are shown in Fig. 3A (b). As compared with the substrate, the coated samples show an increased impedance modulus. PCTyr Schiff base loaded sol-gel coating provides more protection against the corrosion of ZE21B alloy.

3.3.2. In vitro immersion tests and surface morphology

Weight loss results (Fig. 3B) after 3, 7, 14 and 30 days' immersion at 37 °C in SBF were in line with the conclusion drawn in the above electrochemical tests. The two coated samples have a lower corrosion rate than that of the substrate. Compared with the electrochemical data, it can be seen more clearly that the coating loaded corrosion inhibitor further reduces the corrosion rate of Mg. It shows that with the degradation of the sol-gel coating in the corrosive medium, the corrosion inhibitor is released from the coating, with the extension of time, the concentration of inhibitor gradually increases, and its inhibition effect is more obvious, which effectively reduces the degradation rate and suppresses corrosion.

Furthermore, SEM pictures of each specimen surface were also employed to evaluate degradation behavior. Corrosion morphology (without corrosion products) of the bare and coated samples after 7, 14 and 30 days' immersion at 37 °C in SBF is showed in Fig. 3(C). The surface of a corroded bare ZE21B sample is uneven, and it is gully-like, with a large area of corrosion pits, and the corrosion is extremely serious, with the increase of soaking time, this phenomenon is more obvious. For the sol-gel coated ZE21B samples, it could be found that the surface corrosion of the sample is intensified. The corrosion pits are connected with each other, and there is a trendy of deep corrosion. After soaking for 14 days, only a small amount of the sample surface has not been corroded. After soaking for 30 days, the surface of the coating sample is almost completely corroded, but the surface of the coating sample is relatively flat and there is no serious pitting. With the addition of inhibitor, due to the inhibition effect of PCTvr Schiff base, the localized corrosion of the surface of the PCTyr Schiff base sol-gel ZE21B sample which after soaking for 7 days and 14 days is still chain structure, there is less trendy of deep corrosion compared with bare substrate and sol-gel ZE21B samples. on the whole, Samples which soaked for 30 days is still presents relatively uniform corrosion.

3.3.3. Self-healing capacity

To evaluate the self-healing ability for different specimens, the artificial scratch was made on the sol-gel-ZE21B, PCTyr Schiff base solgel ZE21B samples. Fig. 4A (a) shows SEM—EDS of the scratched area of the sol-gel-ZE21B sample after 3 days' immersion. It could be observed that the sol-gel coating samples display micro-cracks and large-scale corrosion pits, indicating severe pitting corrosion. Accordingly, no obvious corrosion pits are observed on the scratched sample coated with PCTyr Schiff base sol-gel, as shown in Fig. 4A (b). On the other hand, SEM image shows no significant corrosion of the substrate around scratch. The corresponding EDS result shows that the corrosion products are mainly composed of C, N, O, Mg, Ca, and Cl elements. Besides, the content of C and N elements in the sample increased significantly and oxygen content decreased significantly compared with the sol-gel-ZE21B sample, which reveals the PCTyr Schiff base-Mg was chelated [54].

When the corrosion products on the surface of the sample are cleaned with chromic acid washing solution, the corrosion morphology can be observed more clearly. From Fig. 4B, when the samples were placed in SBF, the corrosive medium gradually infiltrates between the coating and substrate interface from the damaged part, and the corrosion mainly occurred in the area between the two scratches. With the increase of corrosion time, the corrosion area began to expand from the scratch part, then a large number of corrosion pits appeared, and gradually connected to form a large area of uneven corrosion area, which fails in the barrier effect of the sol-gel coating. At the same time, there is no obvious pitting corrosion around the damaged coating due to the loaded PCTyr Schiff base in the coating. More inhibitors are released from the coating as times go on, the released Schiff base reacts with Mg²⁺ to form complex and deposit on the broken coating, the coating is repaired, and further corrosion is inhibited.

According to the mechanism of the Schiff base inhibitor [54], a possible self-healing mechanism is elucidated in Fig. 4C. Once the sample is immersed in the simulated body fluid, chloride ion penetrates into the magnesium matrix from the damaged part of the coating, and the magnesium matrix is attacked by chloride ion, resulting in local corrosion, and then magnesium ion is released. Meanwhile, as the coating degrades, PCTyr Schiff base released slowly. Then magnesium ion enriched around the alloy surface provides more chance for chelating with PCTyr Schiff base and drives the deposition of PCTyr Schiff base-Mg on the coating defects. The defects of the coating are covered by complex and corrosion products, and a dense protective layer is formed gradually to slow down the further corrosion of chloride ion, which reveals the self-healing mechanism of the PCTyr Schiff base sol-gel coatings.

3.4. Cytotoxicity and proliferation tests

3.4.1. In vitro cytotoxicity tests

Fig. 5A reveals the in vitro cytotoxicity in terms of cell viabilities of the bare ZE21B, sol-gel-ZE21B and PCTyr Schiff base sol-gel ZE21B samples. After 24 h of incubation, compared with the blank control group, the absorbance values of the coating samples and the bare ZE21B samples do not change significantly. However, after 72 h of incubation, the absorbance value of each group increases markedly, and the cell activity increases, but the absorbance value of the bare ZE21B sample is substantially lower than the control group, and the coating sample just slightly lower than that of the control group.

From Table 3, after 24 h of incubation, the cell proliferation rate of the bare ZE21B sample is 85 %, the sol-gel ZE21B sample is 92 %, and PCTyr Schiff base sol-gel ZE21B sample is 88 %. The toxicity gradation of all groups is 1, which reveals that the load of the PCTyr Schiff base in the sol-gel coating has no cytotoxicity. After 72 h of incubation, the cell proliferation rate of the bare ZE21B sample was 77 %, sol-gel ZE21B sample was 85 %, and PCTyr Schiff base sol-gel ZE21B sample was 100 %, the toxicity gradation of PCTyr Schiff base sol-gel ZE21B sample was 0, same as the control group. The results showed that the loading of corrosion inhibitor had no significant effect on the toxicity of the coating, and the two coatings had no toxicity on endothelial cells.

3.4.2. Vascular endothelial cells growth

The rapid endothelialization ability of vascular implants is mainly evaluated by the adhesion and proliferation of endothelial cells. To investigate the endothelial cell growth on ZE21B, sol-gel ZE21B, PCTyr Schiff base sol-gel ZE21B samples, HUVEC were seeded on the surface of each sample. Fig. 5B shows fluorescence images of HUVEC. After 1 d of incubation, we found that most of the HUVEC cells in the two coating groups were round, and the number of HUVEC cells had no significant change compared with the control group, this is due to the short culture time and the incomplete spreading of cells. With the extension of time, the HUVEC cells of all groups gradually spread and proliferated, the density of cells in the bare ZE21B sample was the least, this was owing to

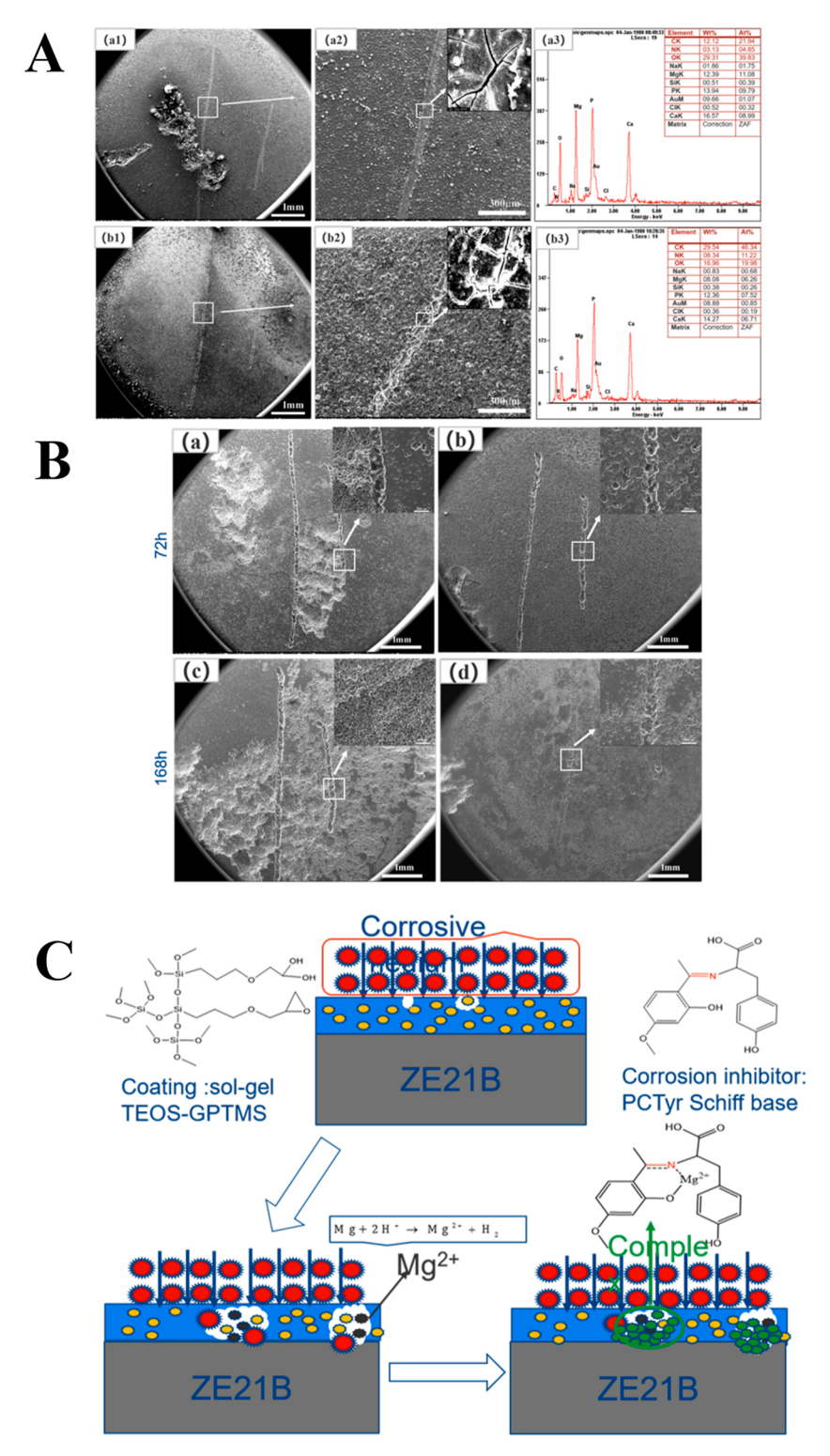


Fig. 4. A SEM-EDS for scratched area of sol-gel coated sample after immersing in SBF solution for 3 days (a sol-gel ZE21B; b PCTyr Schiff sol-gel ZE21B); B SEM images of sample after immersing in SBF solution for (After removing corrosion products; aand c sol-gel ZE21B; b and d PCTyr Schiff sol-gel ZE21B); C Schematic illustration of self-healing mechanism of PCTyr Schiff base sol-gel coating.

the increase of pH caused by the corrosion of the magnesium matrix, which affects the cell adhesion and proliferation. Compared with the bare ZE21B group, the number of cells in the coating group increased significantly, especially in the PCTyr Schiff base sol-gel ZE21B coating group, which even higher than the control group. This indicated that load PCTyr Schiff base in the sol-gel can promote cell proliferation.

In the process of vascular endothelialization, endothelial cells on the

adjacent vascular wall will be induced to migrate to the surface of vascular implant materials. Fig. 6 shows that the scratch healing distance of HUVECs in PCTyr Schiff base sol-gel ZE21B is longer than that in other groups after 36 h, more than 400 μm . This indicates that ZE21B with PCTyr Schiff base in sol-gel coating is more conducive to HUVECs migration.

To explore the mechanism of PCTyr Schiff base beneficial to

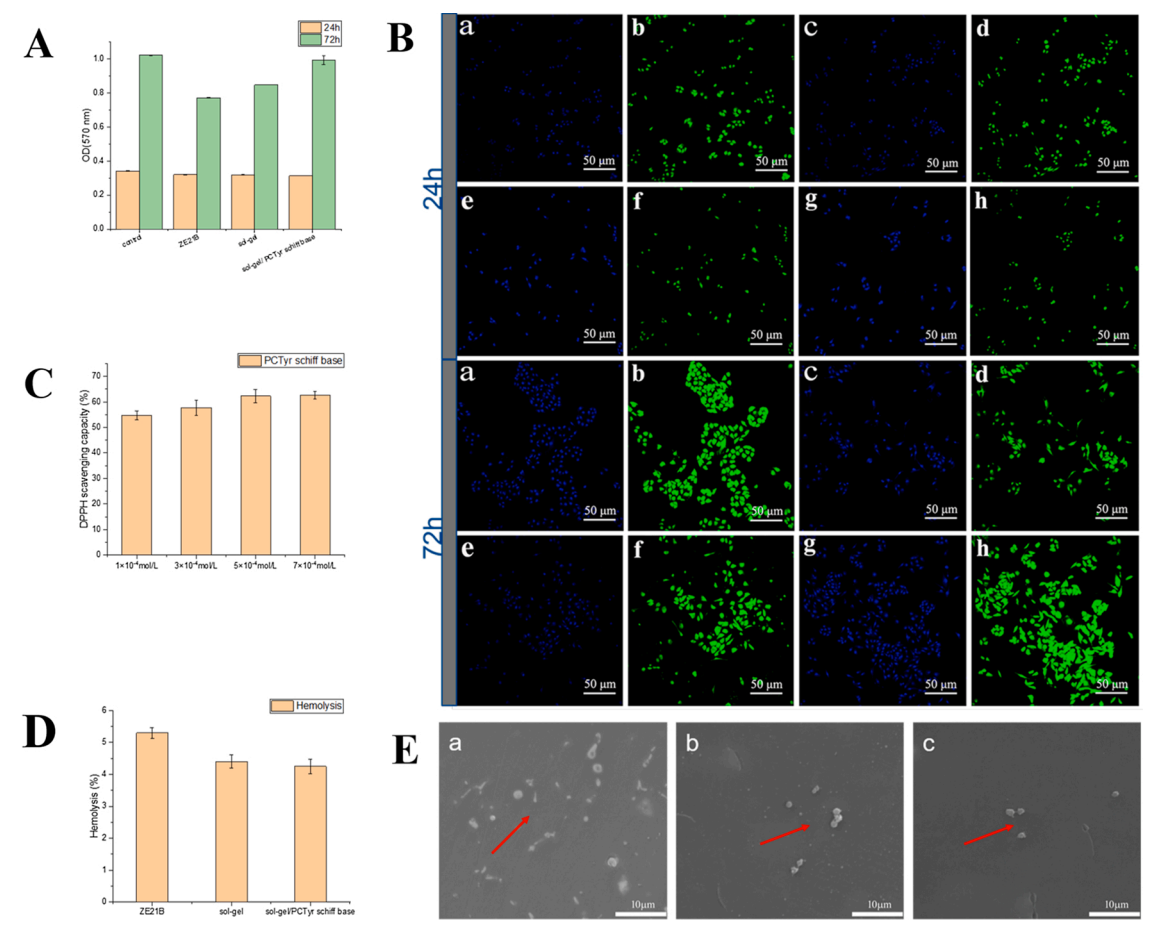


Fig. 5. A Absorbance (OD) of coated sample extract culture cells; B Fluorescence images of HUVEC on samples of control (a, b), ZE21B (c, d), sol-gel ZE21B (e, f) and PCTyr schiff base sol-gel ZE21B (g, h) that stained with rhodamine and DAPI; C DPPH scavenging capacity; D Hemolysis percentage (n = 3); E SEM image of platelet adhesion experiment: ZE21B (a), sol-gel ZE21B(b) and PCTyr schiff base sol-gel ZE21B(c).

Table 3Toxicity rating of coating sample.

	Control	ZE21B	sol-gel	sol-gel/PCTyr Schiff base
24 h RGR /%	100	85	92	88
Toxicity rating	0	1	1	1
72 h RGR /%	100	77	85	100
Toxicity rating	0	1	1	0

endothelial cells, we investigated the DPPH radical scavenging effect of different concentrations of PCTyr Schiff base. As shown in Fig. 5C, the DPPH scavenging ability of PCTyr Schiff base increased with the increase of concentration. Luo et al. [56] reported that the antioxidant function of tea polyphenol (EGCG) can promote the adhesion and proliferation of endothelial cells. Due to its antioxidant capacity similar to EGCG, we believe that the PCTyr Schiff base acts on endothelial cells in the same way.

All the results indicated that the sol-gel layer could significantly ameliorate the endothelialization of ZE21B substrate. Loading PCTyr Schiff base in the sol-gel promoted cell proliferationand further improved the biocompatibility of unique sol-gel coating.

3.5. Blood compatibility

Platelet adhesion is regarded as an essential reaction in response to vascular injury. [19] After the vascular endothelial injury, platelets adhere to the subendothelial matrix and activate. Excessive platelet aggregation and release reaction will lead to thrombosis and eventually

arterial embolism.

The hemolysis rates of bare ZE21B, sol-gel ZE21B, and PCTyr Schiff base sol-gel ZE21B samples after immersed in diluted whole blood for 60 min were exhibited in Fig. 5D. Only the hemolysis rates of the bare ZE21B higher than 5.0 %, the hemolysis rate of the two coating samples was less than 5.0 %, which fully met the requirements of the standard ISO 10993-4:2002 for implantable biomedical materials.

Fig. 5E characterizes the morphology and number of the human platelets assembled onto the surface of each group of ZE21B samples. Compared with coating samples, most platelets adhered on the surface of the bare ZE21B and were almost fully spread, which implied a high degree of platelet activation. The platelet morphology in Fig. 5E showed that platelets presented nearly round shape with no short pseudopodia spreading on the surface of sol-gel ZE21B and PCTyr Schiff base sol-gel ZE21B samples, indicating that the sol-gel coatings load with and without PCTyr Schiff base would not induce the activation of platelets.

Consequently, from the test of the morphology, quantity of adherent platelets, and hemolysis rate, the sol-gel layer loaded with and without PCTyr Schiff base not only has the good characteristics of reducing platelet adhesion, inactivation of platelets but also has an excellent performance in reducing hemolysis rate.

4. Conclusion

The inhibitor-loaded biocompatible sol-gel coating was fabricated on ZE21B alloy by a convenient method, and it yielded the following advantages over the bare ZE21B alloy:

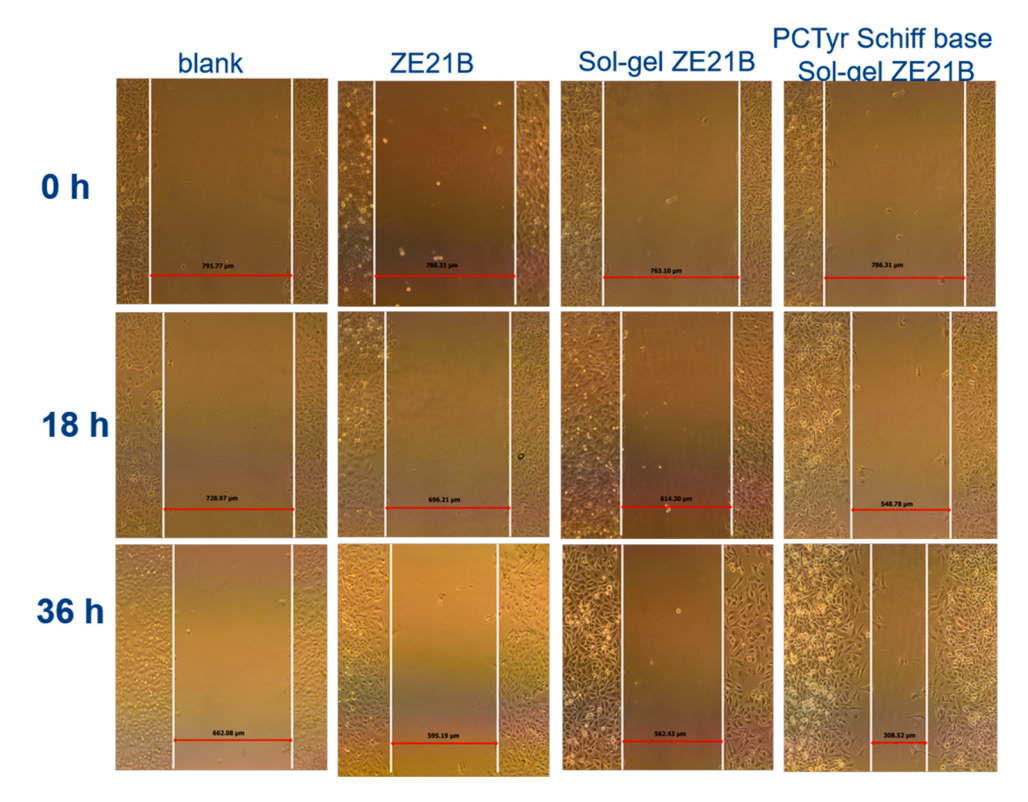


Fig. 6. HUVECs migration experiment: Optical microscopy images at 0 h, 18 h, and 36 h.

- (1) Sol-gel coating loaded with PCTyr Schiff base not only did not destroy the stability of the coating but also increased its corrosion resistance. When the coating was damaged, it also showed selfhealing ability
- (2) The PCTyr Schiff base in the coating had no toxicity on HUVEC cells. It could promote cell proliferation and improve the cell compatibility of the coating. The designed sol-gel coating was biocompatible and also exhibited an anticoagulant effect.
- (3) It was easy to improve the corrosion resistance/biocompatibility and endothelialization of the sol-gel coatings by loading with PCTvr Schiff base inhibitor.
- (4) Through in-depth research, Schiff base inhibitors were expected to replace the drugs in drug-eluting stents and, thus, achieving controllable degradation, improved blood compatibility, and rapid endothelialization, and it could provide a reference for the future coating design and lay a foundation for the clinical application of magnesium alloy biodegradable vascular stent as soon as possible.

Data availability

The raw/processed data required to reproduce these findings cannot be shared at this time as the data also forms part of an ongoing study.

CRediT authorship contribution statement

Weijie Li: Conceptualization, Methodology, Software, Validation, Formal analysis, Data curation, Visualization, Writing - original draft, Writing - review & editing. Ya Su: Methodology, Software, Formal analysis, Data curation. Liang Ma: Methodology, Software, Formal analysis, Data curation. Shijie Zhu: Project administration, Supervision, Resources, Methodology. Yufeng Zheng: Supervision, Writing - review & editing. Shaokang Guan:

Declaration of Competing Interest

The authors declared that they have no conflicts of interest to this work. We declare that we do not have any commercial or associative interest that represents a conflict of interest in connection with the work submitted.

Acknowledgments

The authors are grateful for the financial support of Key Projects of the Joint Fund of the National Natural Science Foundation of China (Grant No: U1804251), the National Key Research and Development Program of China (2018YFC1106703, 2017YFB0702504 and 2016YFC1102403).

Appendix A. Supplementary data

Supplementary material related to this article can be found, in the online version, at doi:https://doi.org/10.1016/j.colsurfb.2021.111993.

References

- C. Campos, T. Muramatsu, J. Iqbal, Y. Zhang, Y. Onuma, H. Garcia-Garcia, et al., Bioresorbable drug-eluting magnesium-alloy scaffold for treatment of coronary artery disease, Int. J. Mol. Sci. 14 (2013) 24492–24500.
- [2] Y. Lu, P. Wan, B. Zhang, L. Tan, K. Yang, J. Lin, Research on the corrosion resistance and formation of double-layer calcium phosphate coating on AZ31 obtained at varied temperatures, Mater. Sci. Eng. C 43 (2014) 264–271.
- [3] S. Wang, X. Zhang, J. Li, C. Liu, S. Guan, Investigation of Mg–Zn–Y–Nd alloy for potential application of biodegradable esophageal stent material, Bioact. Mater. 5 (2020) 1–8.
- [4] M. Liu, J. Wang, S. Zhu, Y. Zhang, Y. Sun, L. Wang, et al., Corrosion fatigue of the extruded Mg-Zn-Y-Nd alloy in simulated body fluid, J. Magnes. Alloy 8 (2020) 231–240.
- [5] L. Mao, L. Shen, J. Niu, J. Zhang, W. Ding, Y. Wu, et al., Nanophasic biodegradation enhances the durability and biocompatibility of magnesium alloys for the next-generation vascular stents, Nanoscale 5 (2013) 9517–9522.
- [6] L. Mao, L. Shen, J. Chen, X. Zhang, M. Kwak, Y. Wu, et al., A promising biodegradable magnesium alloy suitable for clinical vascular stent application, Sci. Rep.-Uk 7 (2017) 46343.

- [7] M. Echeverry-Rendon, F. Echeverria, M.C. Harmsen, Interaction of different cell types with magnesium modified by plasma electrolytic oxidation, Colloids Surf. B Biointerfaces 193 (2020), 111153.
- [8] J. Liu, P. Wang, C. Chu, T. Xi, Arginine-leucine based poly (ester urea urethane) coating for Mg-Zn-Y-Nd alloy in cardiovascular stent applications, Colloids Surf. B Biointerfaces 159 (2017) 78–88.
- [9] X. Gu, Z. Mao, S. Ye, Y. Koo, Y. Yun, T.R. Tiasha, et al., Biodegradable, elastomeric coatings with controlled anti-proliferative agent release for magnesium-based cardiovascular stents, Colloids Surf. B Biointerfaces 144 (2016) 170–179.
- [10] X. Liu, Z. Yue, T. Romeo, J. Weber, T. Scheuermann, S. Moulton, et al., Biofunctionalized anti-corrosive silane coatings for magnesium alloys, Acta Biomater. 9 (2013) 8671–8677.
- [11] P. Lu, H. Fan, Y. Liu, L. Cao, X. Wu, X. Xu, Controllable biodegradability, drug release behavior and hemocompatibility of PTX-eluting magnesium stents, Colloids Surf. B Biointerfaces 83 (2011) 23–28.
- [12] X. Ji, L. Gao, J. Liu, J. Wang, Q. Cheng, J. Li, et al., Corrosion resistance and antibacterial properties of hydroxyapatite coating induced by gentamicin-loaded polymeric multilayers on magnesium alloys, Colloids Surf. B Biointerfaces 179 (2019) 429–436.
- [13] Y. Zhao, X. Chen, S. Li, R. Zeng, F. Zhang, Z. Wang, et al., Corrosion resistance and drug release profile of gentamicin-loaded polyelectrolyte multilayers on magnesium alloys: effects of heat treatment, J. Colloid Interf. Sci. 547 (2019) 309–317.
- [14] Y. Zhao, L. Shi, X. Ji, J. Li, Z. Han, S. Li, et al., Corrosion resistance and antibacterial properties of polysiloxane modified layer-by-layer assembled selfhealing coating on magnesium alloy, J. Colloid Interf. Sci. 526 (2018) 43–50.
- [15] A.A. Ghoneim, A.M. Fekry, M.A. Ameer, Electrochemical behavior of magnesium alloys as biodegradable materials in Hank's solution, Electrochim. Acta 55 (2010) 6028–6035.
- [16] A.M. Fekry, R.H. Tammam, Electrochemical behavior of magnesium alloys as biodegradable materials in phosphate buffer saline solution, Int. J. Electrochem. Sci. 7 (2012) 12254–12261.
- [17] W.M. Hosny, M.A. Ameer, Electrochemical study and biological activity of AZ91E alloy in Hank's solution, Int. J. Electrochem. Sci. 8 (2013) 8371–8387.
- [18] J. Chen, L. Fang, F. Wu, J. Xie, J. Hu, B. Jiang, et al., Corrosion resistance of a self-healing rose-like MgAl-LDH coating intercalated with aspartic acid on AZ31 Mg alloy, Prog. Org. Coat. 136 (2019), 105234.
- [19] D. Liu, E.H. Han, Y. Song, D. Shan, Enhancing the self-healing property by adding the synergetic corrosion inhibitors of Na3PO4 and 2-mercaptobenzothiazole into the coating of Mg alloy, Electrochim. Acta 323 (2019), 134796.
- [20] F. Fan, C. Zhou, X. Wang, J. Szpunar, Layer-by-layer assembly of a self-healing anticorrosion coating on magnesium alloys, ACS Appl. Mater. Inter. 7 (2015) 27271–27278.
- [21] L.M. Calado, M.G. Taryba, M.J. Carmezim, M.F. Montemor, Self-healing ceriamodified coating for corrosion protection of AZ31 magnesium alloy, Corros. Sci. 142 (2018) 12–21.
- [22] H. Su, Y. Liu, X. Gao, Y. Qian, W. Li, T. Ren, et al., Corrosion inhibition of magnesium alloy in NaCl solution by ionic liquid: synthesis, electrochemical and theoretical studies, J. Alloys. Compd. 791 (2019) 681–689.
- [23] A.M. Fekry, M.Z. Fatayerji, Electrochemical corrosion behavior of AZ91D alloy in ethylene glycol, Electrochim. Acta 54 (2009) 6522–6528.
- [24] J. Hu, D. Zeng, Z. Zhang, T. Shi, G. Song, X. Guo, 2-Hydroxy-4-methoxyacetophenone as an environment-friendly corrosion inhibitor for AZ91D magnesium alloy, Corros. Sci. 74 (2013) 35–43.
- [25] A.F. Galio, S.V. Lamaka, M.L. Zheludkevich, L.F.P. Dick, I.L. Müller, M.G. S. Ferreira, Inhibitor-doped sol-gel coatings for corrosion protection of magnesium alloy AZ31, Surf. Coat. Technol. 204 (2010) 1479–1486.
- [26] N.H. Helal, W.A. Badawy, Environmentally safe corrosion inhibition of Mg-Al-Zn alloy in chloride free neutral solutions by amino acids, Electrochim. Acta 56 (2011) 6581-6587
- [27] D. Huang, J. Hu, G. Song, X. Guo, Inhibition effect of inorganic and organic inhibitors on the corrosion of Mg-10Gd-3Y-0.5Zr alloy in an ethylene glycol solution at ambient and elevated temperatures, Electrochim. Acta 56 (2011) 10166-10178.
- [28] R. Supplit, T. Koch, U. Schubert, Evaluation of the anti-corrosive effect of acid pickling and sol-gel coating on magnesium AZ31 alloy, Corros. Sci. 49 (2007) 3015–3023.
- [29] L. Hou, N. Dang, H. Yang, B. Liu, Y. Li, Y. Wei, et al., A combined inhibiting effect of sodium alginate and sodium phosphate on the corrosion of magnesium alloy AZ31 in NaCl solution, J. Electrochem. Soc. 163 (2016) C486–94.
- [30] L. Yang, Y. Li, B. Qian, B. Hou, Polyaspartic acid as a corrosion inhibitor for WE43 magnesium alloy, J. Magnes. Alloy. 3 (2015) 47–51.
- [31] S.V. Lamaka, B. Vaghefinazari, D. Mei, R.P. Petrauskas, D. Höche, M. L. Zheludkevich, Comprehensive screening of Mg corrosion inhibitors, Corros. Sci. 128 (2017) 224–240.

- [32] G. Song, D.H. StJohn, Corrosion of magnesium alloys in commercial engine coolants, Mater. Corros. 56 (2005) 15–23.
- [33] J.Y. Hu, X.Q. Song, Z. Zhang, D.Z. Zeng, T.H. Shi, J.F. Gao, The corrosion inhibition behaviors of 2'-hydroxy-acetophenone for AZ91D magnesium alloy, Mater. Corros. 66 (2015) 396–404.
- [34] D. Daloz, C. Rapin, P. Steinmetz, G. Michot, Corrosion inhibition of rapidly solidified Mg-3% Zn-15% Al magnesium alloy with sodium carboxylates, Corrosion-Us. 54 (1998) 444–450.
- [35] A. Frignani, V. Grassi, F. Zanotto, F. Zucchi, Inhibition of AZ31 Mg alloy corrosion by anionic surfactants, Corros. Sci. 63 (2012) 29–39.
- [36] D. Huang, Y. Tu, G. Song, X. Guo, Inhibition effects of Pyrazine and Piperazine on the corrosion of Mg-10Gd-3Y-0.5Zr alloy in an ethylene glycol solution, Am. J. Analyt. Chem. 04 (2013) 36–38.
- [37] Y. Dai, Q. Li, H. Gao, L.Q. Li, F.N. Chen, F. Luo, et al., Effects of five additives on electrochemical corrosion behaviours of AZ91D magnesium alloy in sodium chloride solution, Surf Eng. 27 (2013) 536–543.
- [38] P. Lu, H. Fan, Y. Liu, L. Cao, X. Wu, X. Xu, Controllable biodegradability, drug release behavior and hemocompatibility of PTX-eluting magnesium stents, Colloids Surf. B Biointerfaces 83 (2011) 23–28.
- [39] J. Liu, B. Zheng, P. Wang, X. Wang, B. Zhang, Q. Shi, et al., Enhanced in vitro and in vivo performance of Mg–Zn–Y–Nd alloy achieved with APTES pretreatment for drug-eluting vascular stent application, ACS Appl. Mater. Inter. 8 (2016) 17842–17858.
- [40] Y. Shi, L. Zhang, J. Chen, J. Zhang, F. Yuan, L. Shen, et al., In vitro and in vivo degradation of rapamycin-eluting Mg-Nd-Zn-Zr alloy stents in porcine coronary arteries, Mater. Sci. Eng. C 80 (2017) 1–6.
- [41] M. Haude, H. Ince, S. Kische, R. Toelg, N.M. Van Mieghem, S. Verheye, et al., Sustained safety and performance of the second-generation sirolimus-eluting absorbable metal scaffold: pooled outcomes of the BIOSOLVE-II and -III trials at 3 years, Cardiovasc. Revascul. Med. 21 (2020) 1150–1154.
- [42] M. Kopacz, S. Kopacz, E. Skuba, Redox reactions of quercetin and quercetin-5'-sulfonic acid with Fe³⁺ and Cu²⁺ ions and with H₂O₂, Russ. J. Gen. Chem. 74 (2004) 957–959.
- [43] M. Köse, G. Ceyhan, M. Tümer, O. Demirtaş, O. Gönül, V. McKee, Monodentate Schiff base ligands: their structural characterization, photoluminescence, anticancer, electrochemical and sensor properties, Spectrochim. Acta A. Mol. Biomol. Spectrosc. 137 (2015) 477–485.
- [44] D. Mei, S.V. Lamaka, X. Lu, M.L. Zheludkevich, Selecting medium for corrosion testing of bioabsorbable magnesium and other metals a critical review, Corros. Sci. 171 (2020), 108722.
- [45] Y. Feng, S. Zhu, L. Wang, L. Chang, B. Yan, X. Song, et al., Characterization and corrosion property of nano-rod-like HA on fluoride coating supported on Mg-Zn-Ca alloy, Bioact. Mater. 2 (2017) 63–70.
- [46] P. Xiong, Z. Jia, W. Zhou, J. Yan, P. Wang, W. Yuan, et al., Osteogenic and pH stimuli-responsive self-healing coating on biomedical Mg-1Ca alloy, Acta Biomater. 92 (2019) 336–350.
- [47] L. Chen, J. Li, J. Chang, S. Jin, D. Wu, H. Yan, et al., Mg-Zn-Y-Nd coated with citric acid and dopamine by layer-by-layer self-assembly to improve surface biocompatibility, Sci. China Ser. E Technol. Sci. 61 (2018) 1228–1237.
- [48] Y. Yu, S. Zhu, Y. Hou, J. Li, S. Guan, Sulfur contents in sulfonated hyaluronic acid direct the cardiovascular cells fate, ACS Appl. Mater. Inter. 12 (2020) 46827–46836.
- [49] S.V. Lamaka, D. Höche, R.P. Petrauskas, C. Blawert, M.L. Zheludkevich, A new concept for corrosion inhibition of magnesium: suppression of iron re-deposition, Electrochem. Commun. 62 (2016) 5–8.
- [50] D.K. Ivanou, K.A. Yasakau, S. Kallip, A.D. Lisenkov, M. Starykevich, S.V. Lamaka, et al., Active corrosion protection coating for a ZE41 magnesium alloy created by combining PEO and sol-gel techniques, RSC Adv. 6 (2016) 11256–12553.
- [51] S.V. Lamaka, G. Knörnschild, D.V. Snihirova, M.G. Taryba, M.L. Zheludkevich, M. G.S. Ferreira, Complex anticorrosion coating for ZK30 magnesium alloy, Electrochim. Acta 55 (2009) 131–141.
- [52] D. Höche, C. Blawert, S.V. Lamaka, N. Scharnagl, C. Mendis, M.L. Zheludkevich, The effect of iron re-deposition on the corrosion of impurity-containing magnesium, Phys. Chem. Chem. Phys. 18 (2016) 1279–1291.
- [53] M.F. McCarty, Complementary vascular-protective actions of magnesium and taurine: a rationale for magnesium taurate, Med. Hypotheses 46 (1996) 89–100.
- [54] L. Ma, W. Li, S. Zhu, L. Wang, S. Guan, Corrosion inhibition of Schiff bases for Mg-Zn-Y-Nd alloy in normal saline: experimental and theoretical investigations, Corros. Sci. (2021), 109268.
- [55] Y.T. Caballero, E.A. Rondón, L. Rueda, C.A. Hernández Barrios, A. Coy, F. Viejo, Corrosion resistance of multilayer hybrid sol-gel coatings deposited on the AISI 316L austenitic stainless steel, J. Phys. Conf. Ser. 687 (2016) 12014.
- [56] B. Zhang, R. Yao, L. Li, Y. Wang, R. Luo, L. Yang, et al., Green tea polyphenol induced Mg2+ -rich multilayer conversion coating: toward enhanced corrosion resistance and promoted in situ endothelialization of AZ31 for potential cardiovascular applications, ACS Appl. Mater. Inter. 11 (2019) 41165–41177.